Penerbit Akademia Baru

Journal of Advanced Research in Fluid Mechanics and Thermal Sciences

Journal homepage: www.akademiabaru.com/arfmts.html
ISSN: 2289-7879

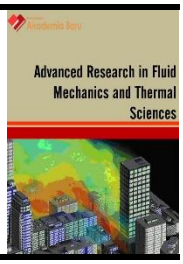

Studying the Effect of Geometric Parameters of Axial Fan Twisted Blades Inside Different Cross-Sectional Ducts

Open Access

Mustafa Ahmed Abdulhussain[1,*]

[1] Department of Mechanical Engineering, University of Technology, Baghdad, Iraq

ARTICLE INFO

Article history:
Received 19 October 2019
Received in revised form 16 November 2019
Accepted 1 December 2019
Available online 26 January 2020

ABSTRACT

Numerical simulation validated with experimental tests is carried out to study the effects of changing some geometrical parameters concerning the twisted blades of a DC power driven computer-case axial fan having a curved-shape winglet tip including the winglet tip mean bending angle, the winglet tip height and the blade profile leading-edge twisting angle. The winglet tip incidence angle is changed from (90-70) degrees, the blade tip base height is increased by (10) %, and the variation of the blade twisting angle is changed from (35-24) degrees considering the air flow past the rotating fan is isothermal and subsonic, the simulation is performed using the shear stress incorporated K-ω turbulence model in the ANSYS-CFX package neglecting the thermal effect considering the flow is passing through rectangular and circular cross-sectional ducts. The results indicated that the fan is more effective using the circular duct regarding that the three investigated parameters have a differential influence on the free stream flow.

Keywords:
Winglet fan; round and square ducts; CFD simulation

1. Introduction

The blades tips changing configurations were considered one of the most efficient methods for decreasing the flow disturbances, the induced drag and the flow noise level for the flow [1] behind the air foiled shapes such as the wings and the rotating fans, the useful rise of the flow velocity and the coefficient of lift as well as the minimization of the secondary leakage in addition to the blade tip generated vortices is achieved through the utilization of the grooved tips and the winglet tips [2] axial flow fans.

One of the geometrical parameters concerning the winglet blade is the incident (or bending) angle effect of the suction side winglet for NACA 0012 blade profile 3D wing is investigated by Belferhat *et al.,* [3] experimentally to evaluate the lift and the induced drag coefficients at flow velocities from 20-40 m/sec in an open type wind tunnel, the study included the change of incidence from 55˚C to 75˚C. The calculations based on the experimental data showed that the winglet has a

* *Corresponding author.*
E-mail address: mustafa_ahmed2018@yahoo.com (Mustafa Ahmed Abdulhussain)

positive effect on the aerodynamic wing performance denoting that the 55˚C is the optimum performance incidence angle.

Shaobing *et al.,* [4] studied experimentally the effect of the winglet tip utilization on the subsonic flow pattern around an eight row NACA 65 axial compressor cascade, the investigation included the application of three different models of blade tip arrangement; the baseline side, the suction side and the pressure side tips considering variable blade incidence angle between -2.5 to 8.5˚C. The experimental results showed that the suction side winglet tip provides the lowest flow pressure loss as compared with the baseline and the pressure line tips. In addition, the incidence angle variation is a high affecting parameter on the formulation shape of the blade tip generated vortices.

The axial fan performance enhancement by applying the winglet tip to reduce the tip clearance flow losses is investigated by Chan *et al.,* [5] numerically and experimentally, the application of the winglet have minimized the flow leakage and the formulation of secondary flow vortices in addition to the improvement in the fan capacity and the air pressure distribution.

The utilization of both suction and pressure sides winglet blades in the reversed axial fan with variable span blade profile is simulated by Beskales *et al.,* [6] for incompressible air flow using the RNG K-ε model, The results showed an observed rise in the flow velocity components when the winglet tip is utilized as well as the winglet contributes to reducing the leakage flow, also the fan efficiency is increased from 3.5-6% depending on the desired design point. The fan efficiency change and the flow evaluated total pressure with increased inlet mass flow rate was validated and indicated a good agreement with previous experimental work.

Jung and Joo [7] studied numerically the effect of the winglet tip clearance on the leakage mass flow rate for the swept-back shrouded axial fan having winglet height and tip clearance distances equals to 3.8 and 3.2% of the blade radius using the Navier-Stokes equations and the SST K-ω turbulence model, they concluded that the optimum winglet tips clearance that produces the maximum fan efficiency occurs with shroud height equals 30% of the fan blade chord length for a certain value of tip clearance (not equal to zero) and the fan efficiency is increased by 10%. The comparison with experimental tests leads to the adoption of the above prescribed numerical method that gives high results accuracy.

Bizjan *et al.,* [8] implemented experimental testing to evaluate the axial fan efficiency and noise level through the measuring of the velocity and pressure fluctuations in the blades tip region. The winglet configuration achieved a streamed transition of flow between the fan blades surfaces. The numerical solution techniques for the flow inside various shape ducts is tested by several researchers; Gavrilov and Rudyak [9] simulated numerically the fully developed flow in circular pipe using the multi-block structured grid for the range of Reynolds number (10000-20000), the applied solution method achieved a good agreement with the experimental tests concluded correlations.

Volkov [10] investigated the unstructured grid dependency near the walls on the flow domain inside the low speed compressor internal mid-blade with the adoption of the control volume solution method using three turbulent models; the Spalart-Allmaras, the K-ε, and the two layer models. He concluded that the grid resolution near the blade trailing edge and the method of connection of the structured mesh near the boundary layer will influence the numerical accuracy results.

Circular and rectangular cross-sectional ducts separated flow simulation is performed by Connolly and Loth [11] using the detached eddy simulation turbulence model and implementing 5 million structured grid, the circular duct flow results gives a great match with previous experimental work for instantaneous results, on the other hand the rectangular duct flow separation is lower than the circular type. The Numerical solution for the unsteady symmetrical flow past a rotating body is performed by Demenkov and Chernykh [12], they developed a mathematical model that is based on the Reynolds stress turbulence model with applying first order finite difference solution algorithm

that is applicable for the swirling past flow, the results indicated that the flow past the rotating body becomes entirely shear less.

The aim of this research is to investigate numerically using the ANSYS CFX code the flow velocity pattern inside circular and square cross-sectional ducts accelerated by a DC-driven small axial fan with curved winglet tip operating with its design rotational velocity (1500 RPM), the study will include the effect of changing several winglet characteristics such as the tip bending angle from 90-70˚C in addition to the winglet tip maximum height change within 10% of the base height, and also the variation effect of the blade end tip twisting angle from 35˚C to 24˚C.

2. Problem Statement

The studying of the rotating axial fan with winglet tips blades surface-geometrical parameters for the accelerated flow characteristics in both circular and square cross-sectional ducts including the variation of the winglet incidence (bending) angle, the maximum winglet tip height and the fan blade profile leading edge slope (twisting) angle via numerical simulation using the ANSYS CFX code and validated with experimental test for the fan original shape configuration. The fan base model illustrated in Figure 1 (a)-(d) represents a DC power driven axial fan with nine radial shaped blades made from polystyrene containing curved winglet tips with main dimensions are shown in Table 1, the three proposed modifications to the fan blades geometry are investigated by the following recital; first the mean winglet incidence angle is reduced from 90˚C to both 80˚C and 70˚C separately, second for the modified shape blades the winglet tip height is increased by 10% , and finally the blade profile mean chord twisting angle (28°) revealed in Figure 1 (c) has changed to 35˚C, 30˚C, 26˚C and 24˚C, respectively.

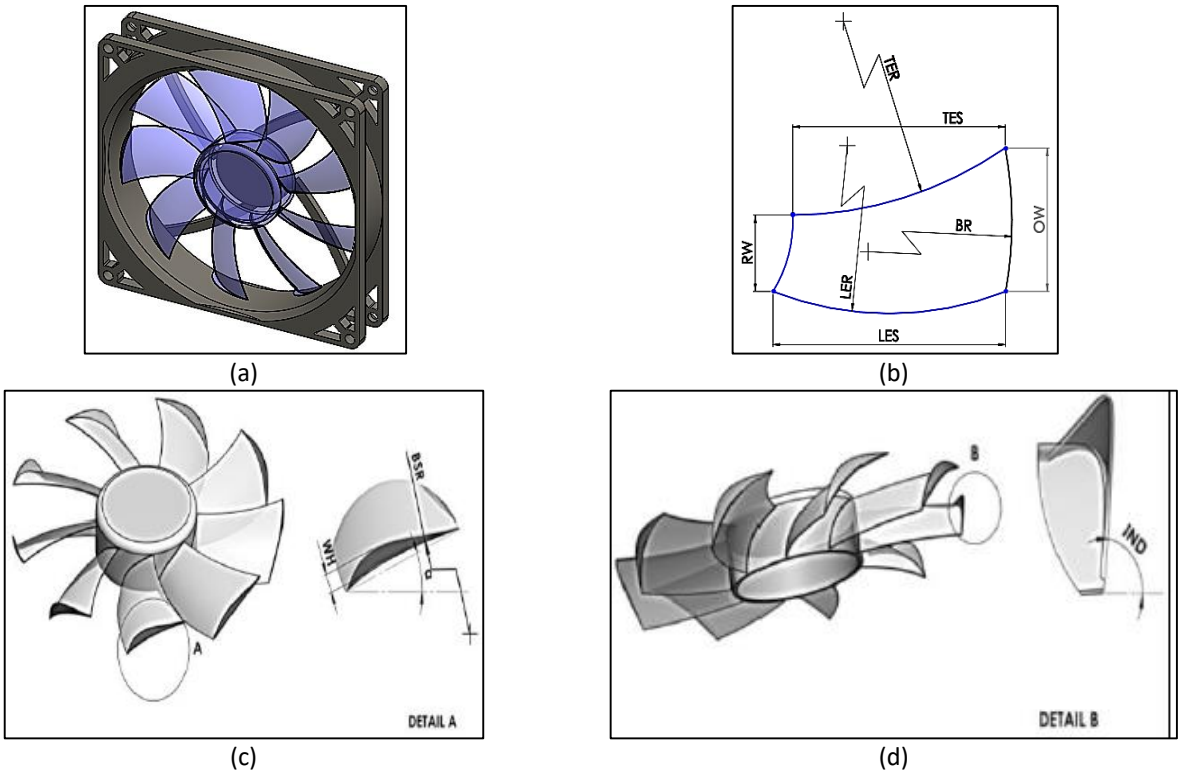

Fig. 1. The fan base model illustrated in various view; (a) winglet axial fan general view (b) fan blade top view (c) blade winglet front curvature angles and (d) blade tip side incidence angle

Table 1
Axial fan geometry characteristics

Symbol	Definition	Value
a	Blade tip twist angle	28° (default)
BR	Blade outer width	11.5 mm
BSR	Blade suction radius	3.4 mm
IND	Blade tip incidence angle	90° (default)
LER	Leading edge radius	58 mm
LES	Leading edge span	38.5 mm
OW	Blade outer width	21.6 mm
RW	Blade root width	11.5 mm
TER	Trailing edge radius	66.25 mm
TES	Trailing edge span	35 mm
WH	Winglet maximum tip height	3 mm

3. Methodology

The mathematical model most utilized for solving the winglet fixed aerofoil parts is the Reynolds Navier-Stokes equations and the Shear stress turbulence model using the finite volume method. The incorporation of the moving boundary cases involving the rotodynamic devices requires careful selection for the turbulence model since it deals with precise and limited fan blades profile changes. The shear stress K-ω turbulence model achieved a desirable computational solution accuracy for the axial and tangential velocity components especially near the wall for low Reynolds number flows [13] where this model utilization requires precise grid mesh [14] for the flow involved streamlined curvature flows.

The kinetic energy transport equation

$$\frac{\partial}{\partial t}(\rho k)+\frac{\partial}{\partial x}(\rho k u)=\frac{\partial}{\partial x}\left\{A_k\frac{\partial k}{\partial x}\right\}+B_k-Y_k+S_k \tag{1}$$

The vorticity transport equation

$$\frac{\partial}{\partial t}(\rho \omega)+\frac{\partial}{\partial x}(\rho \omega u)=\frac{\partial}{\partial x}\left\{A_\omega\frac{\partial \omega}{\partial x}\right\}+B_\omega-Y_\omega+S_\omega \tag{2}$$

where the terms A_k and A_w are the effective diffusivity for the flow kinetic energy (k) and its rate of dissipation (ω), B_k and B_w are the rate of generation for K & ω. The terms Y_k and Y_w represents the turbulence dissipation of k and ω.

In order to achieve an accurate solution for the defined problem, the implementation of the K-ω regime to the SST model as an advanced turbulence control is applied by adding the eddy diffusivity turbulent flux closure option.

3.1 The Numerical Solution Mesh

The adoption of the curvature size mesh tetrahedrons method with the high smoothing and the fast transition criteria in addition to the high span centre angle selection defining the maximum inflation layers to 5 and setting the transition ratio to 0.77 with the assigning of the unstructured mesh growth rate by its default value 1.2 achieved a precise unstructured computational mesh that reached more than 6 million nodes and 4 million elements as illustrated in Figure 2.

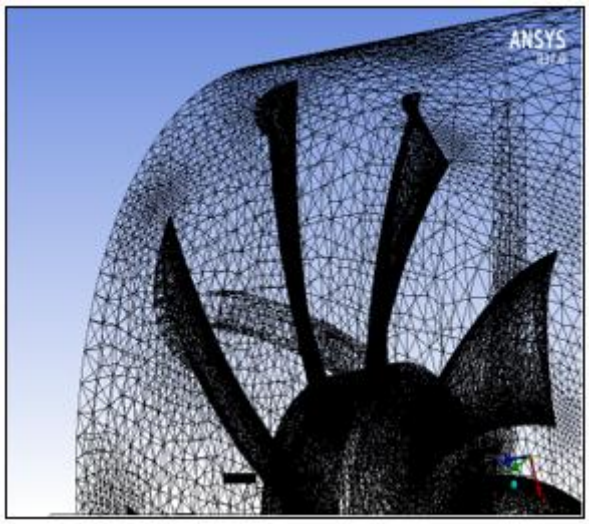

Fig. 2. The flow domain computational mesh

3.2 The Solution Algorithm

The transient time stepping algorithm using the second order backward Euler with the high-resolution scheme is adopted for the cases simulation using either circular or square cross-sectional area mini-ducts shown in Figure 3 (a) and 3 (b) with 0.5 s time step integral with the setting of the continuity, momentum and the turbulence equations conservation target to ($1e^{-3}$), the relatively mesh displacement to the previous time step is adopted for the fluid mesh deformation with increased mesh stiffness near the smallest volumes. The interface between the fan solid and the air-fluid bodies is set to the general connection model defining the interfaced mesh as a surface of revolution to the locally defined z-coordinate.

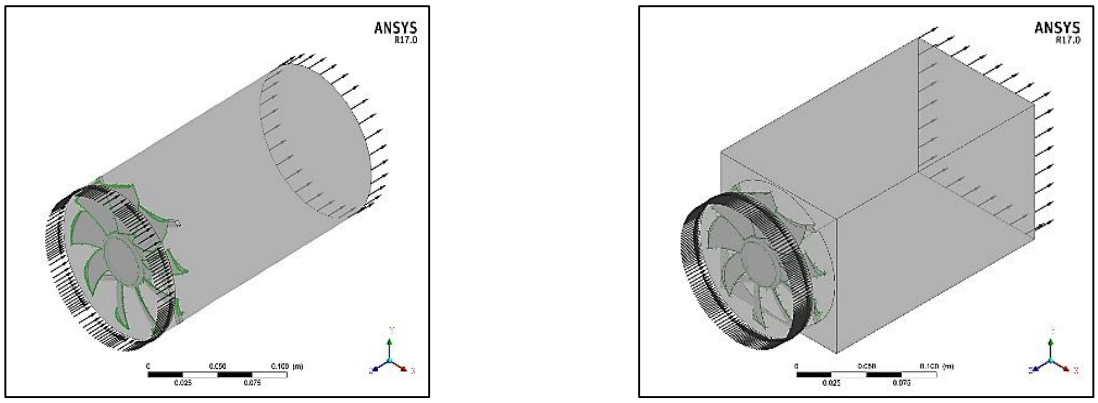

(a) (b)

Fig. 3. Cases simulation in (a) circular duct simulation domain and (b) square duct simulation domain

3.3 Experimental Arrangement

The accelerated flow past the DC driven small model axial fan with its default designed blades are placed at the entrance of the perforated shape mini-ducts with a 4mm thickness having total length 20 cm. The validation of the accelerated flow velocity contours is obtained though the utilization of 1/8 inch size stainless steel Pitot tube model no. 166-12-CF. The measuring device is

oriented linearly at two different locations along the duct length as shown in Figure 4 (a) and 4 (b), for each specified location the Pitot tube reading position is taken at six vertical points at the mid-fan location. The first longitudinal Pitot tube position is located 1 cm after the fan body, and the second is located 3 cm downstream the duct length.

(a)

(b)

Fig. 4. Pitot tube in axial (a) and (b) circumferential reading position

4. Results

4.1 The Winglet Incidence Angle

After reaching the conservation target for the solution of the governing equations, the axial velocity magnitude (u) at the mid-circular duct width shown in Figure 5 (a)-(c) represents the effect of variation of the blade tip incidence (bending) default designed value from 90˚C to 80˚C and 70˚C, respectively. The effect of decreasing the blade tip incidence shows a gradual increase of velocity at the propeller region that diminishes linearly with duct length noticing that the 90° incidence achieves more stable near-wall velocity degradation in the longitudinal direction; this is due to the minimized effect of the wall reduced tip clearance.

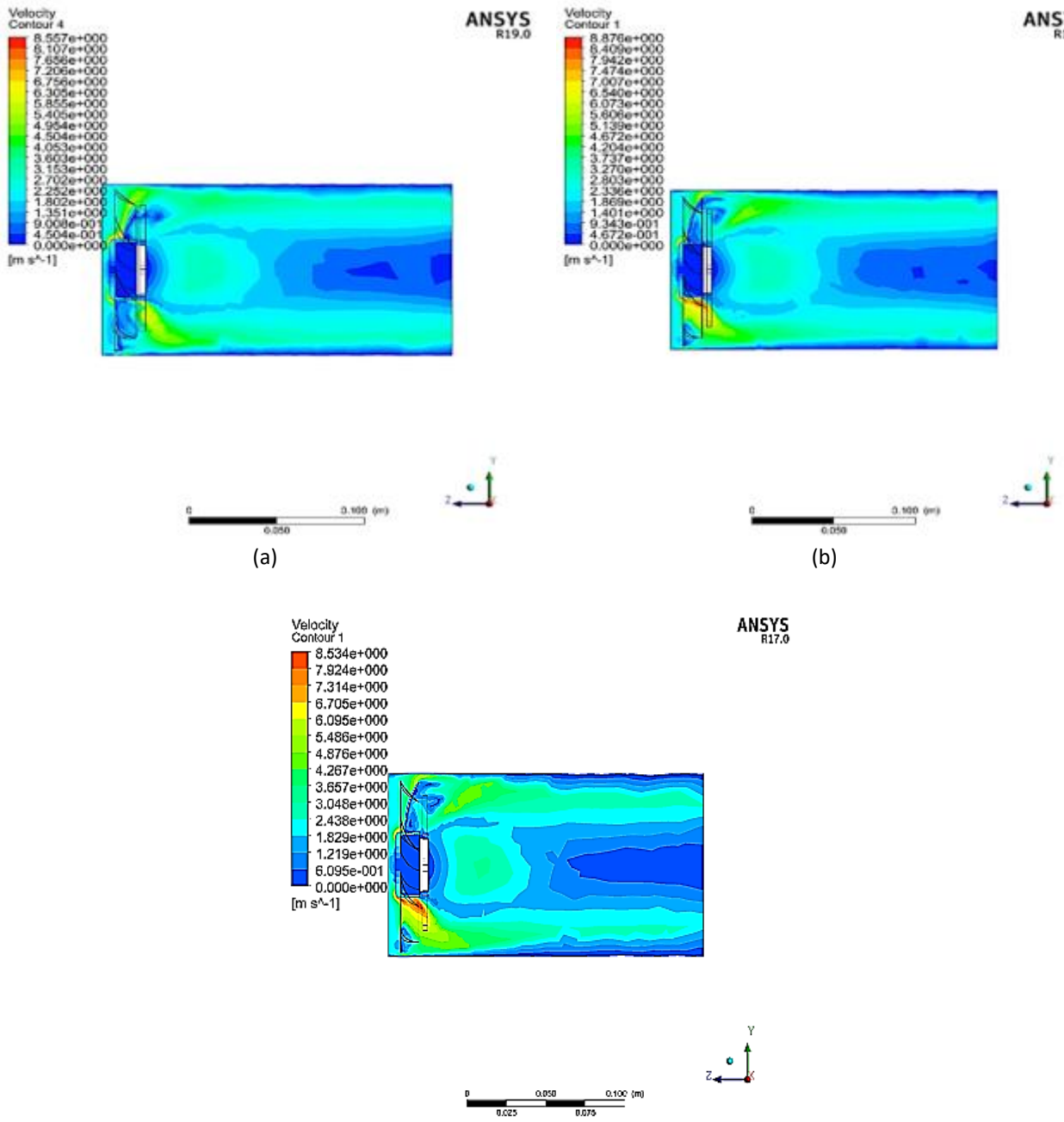

Fig. 5. Axial flow velocity contour for (a) IND=90 (b) IND=80 and (c) IND=70˚C

In the normal direction to the flow located between the fan propeller and the fan, the case supports inside the circular duct as browsed in Figure 6 (a)-(c), the incidence change effect on the velocity distribution denotes increased velocity flow near the tip of the blade since the near-wall region is gradually raised, the flow field adjacent to the blades gaps is relatively slowed especially near the winglet tip owing to increased secondary flow vortices at the winglet tip corners.

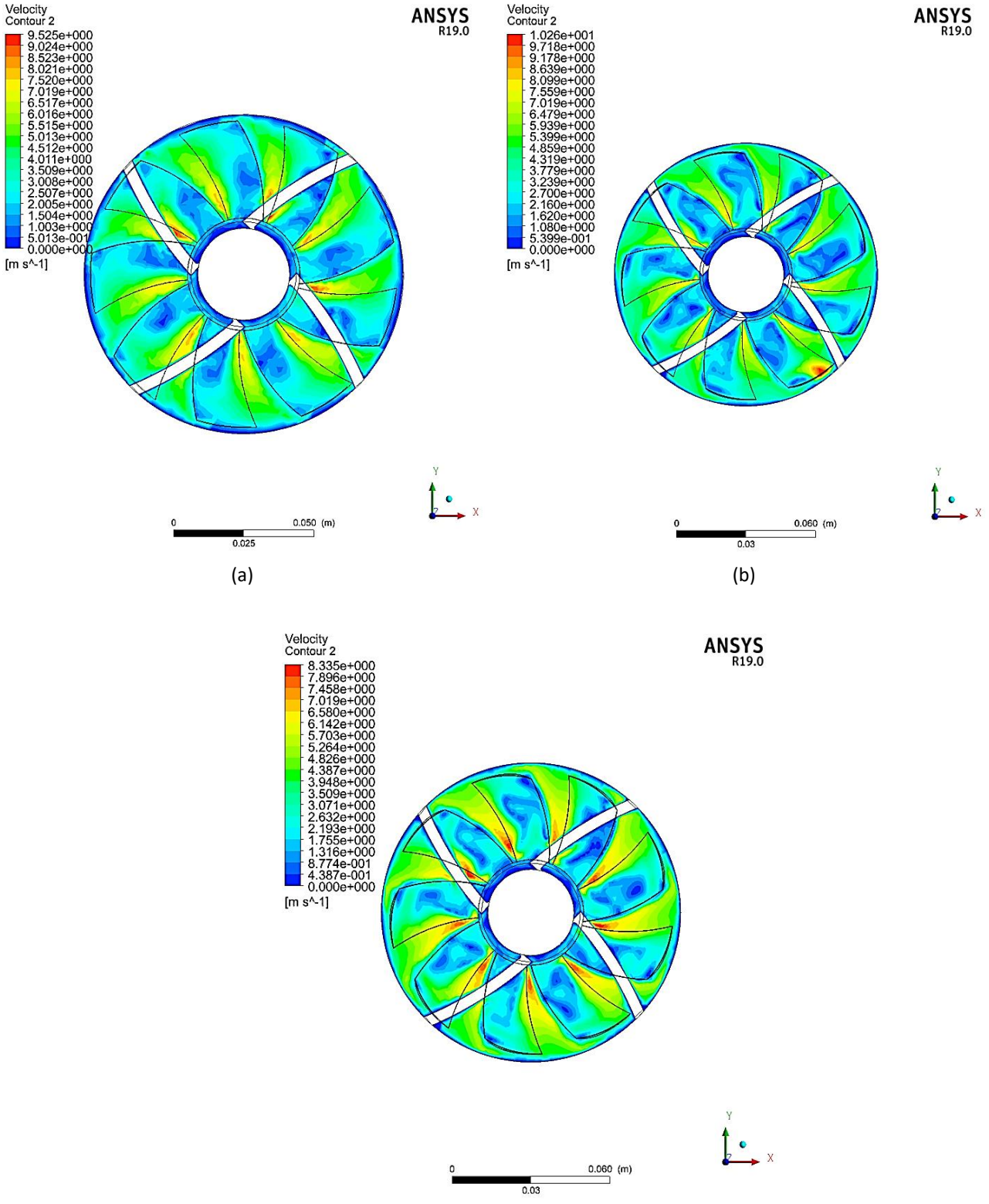

Fig. 6. Velocity contour for (a) IND=90 (b) IND=80 and (c) IND=70˚C

The simulation velocity contours for the same longitudinal location inside the square shape duct illustrated in Figure 7 (a)-(c) indicated a rapid depression near the blade tip region and semi-continuous episodes of accelerated flow at the same region that is gradually dropped in their maximum value with the incidence angle decrement due to the same above mentioned reasons.

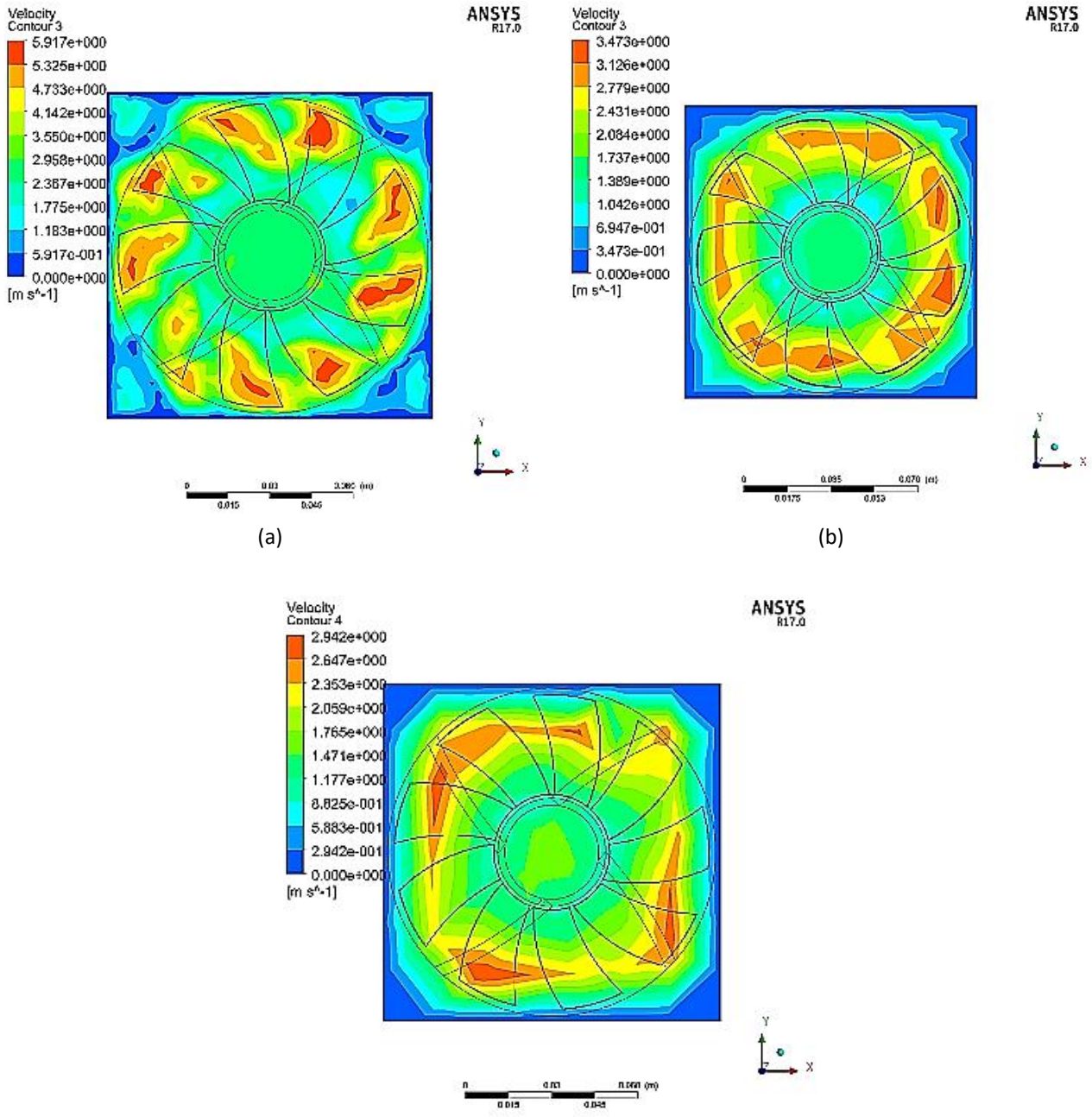

Fig. 7. Velocity contour for (a) IND=90 (b) IND=80 and (c) IND=70˚C

4.2 The Blade Tip Height Variation

The Blade winglet tip default height 3 mm increment by a maximum of 10% is performed through the thickening of the suction side blade curvature profile by the desired amount reaching peak thickness of 3.3 mm without the change of the blade leading edge radius. The simulated results illustrated in Figure 8 (a)-(c) are the sum of the dual effect of changing both the blades tip height 90-70˚C in addition to the blades profile maximum height, the small reduction of the streamline flow velocity as compared with the original fan blade height previous results in Figure 5 (a)-(c) indicates their small effect on the winglet turbulence reduction.

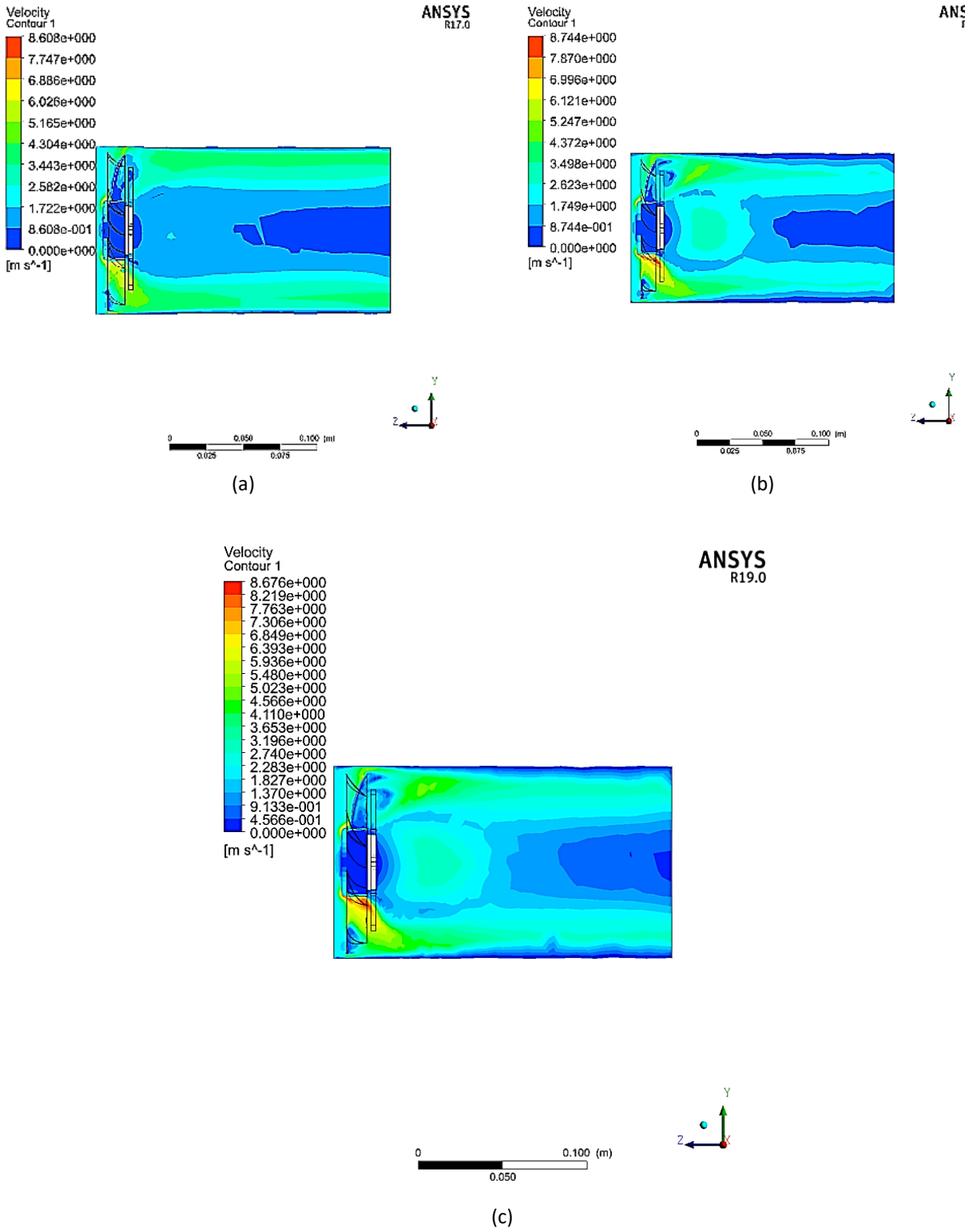

Fig. 8. Velocity contour for (a) IND=90 (b) IND=80 and (c) IND=70˚C for the modified winglet height

The vertical orientation V-contour view for the combination effect of both the winglet tip height and the incidence angle just after the fan propeller previewed in Figure 9 (a)-(c) denotes that the vertical alignment of the tip of the blade achieves the most homogeneous velocity contour with less near- zero velocity gradient since the vertical incidence will cause more secondary uniform flow that will be traversed tangentially as the fan rotates.

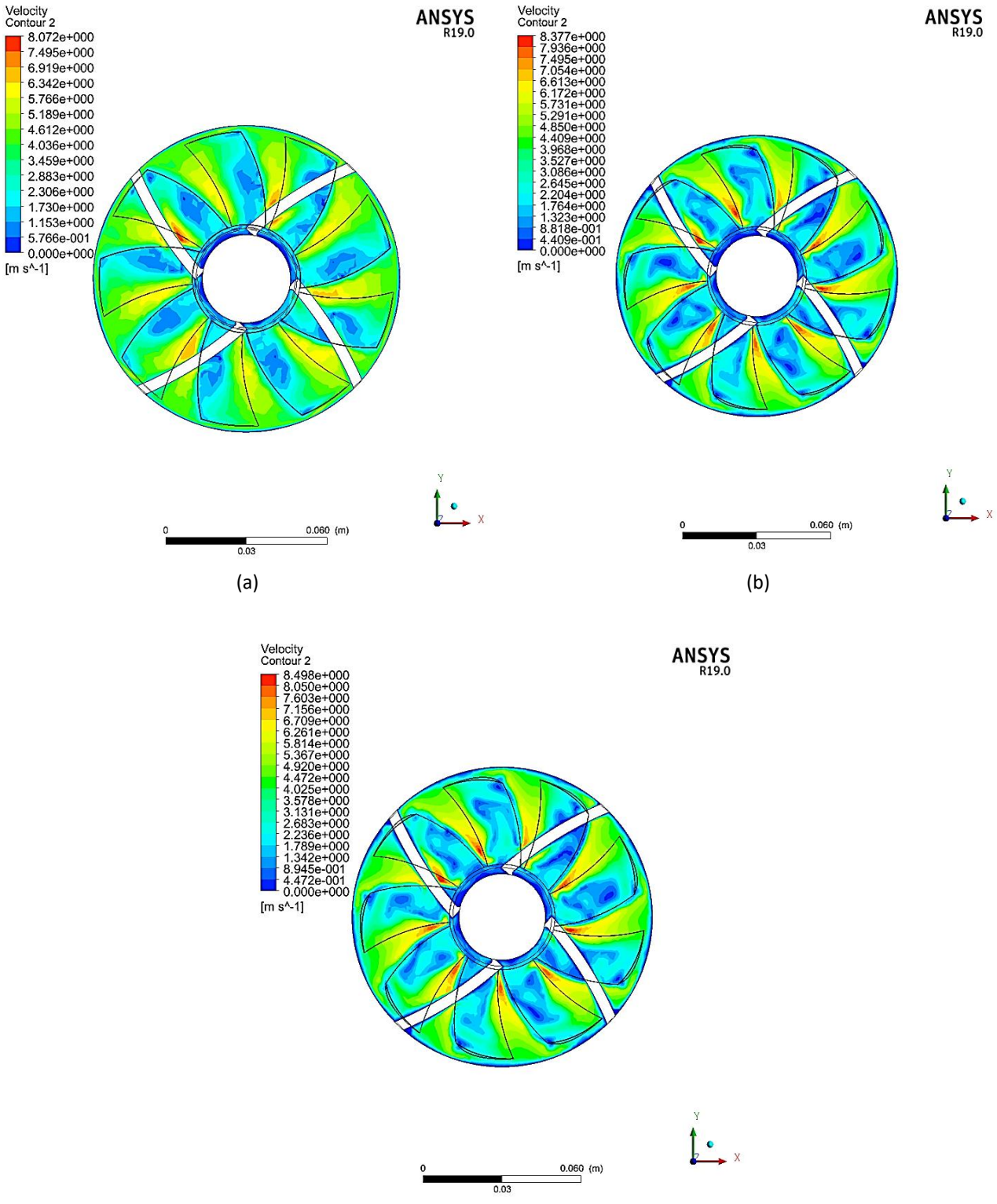

Fig. 9. Velocity contour for (a) IND=90 (b) IND=80 and (c) IND=70˚C for the modified winglet height

A similar effect is monitored in Figure 10 (a)-(c) when the pre-mentioned parameters are investigated when utilizing the fan in the square type duct but with a lower velocity gradient remarking the winglet tip maximum accelerating regions are suddenly dropped with the change of the vertical tip alignment condition for the same mentioned reason.

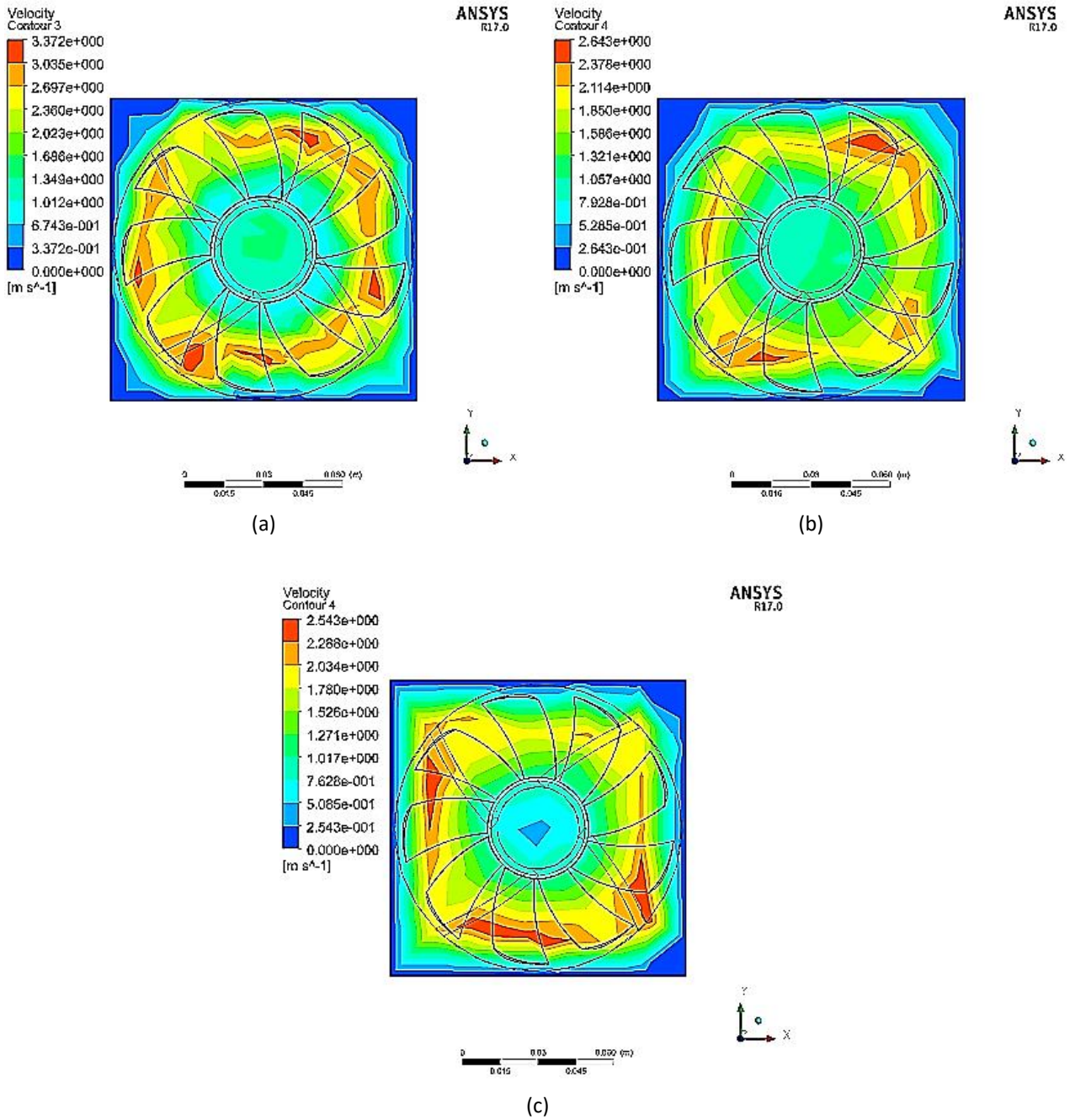

Fig. 10. Velocity contour for (a) IND=90 (b) IND=80 and (c) IND=70˚C for the modified winglet height

4.3 The Fan Blade Twisting Angle Effect

As indicated from the Figure 11 (a)-(e), the change in the blades profile twist angle from 35˚C to 24˚C causes gradual growth of retracted flow wakes region behind the fan propeller in the longitudinal direction with no real significance for the free stream velocity adjacent to the fan blades profiles.

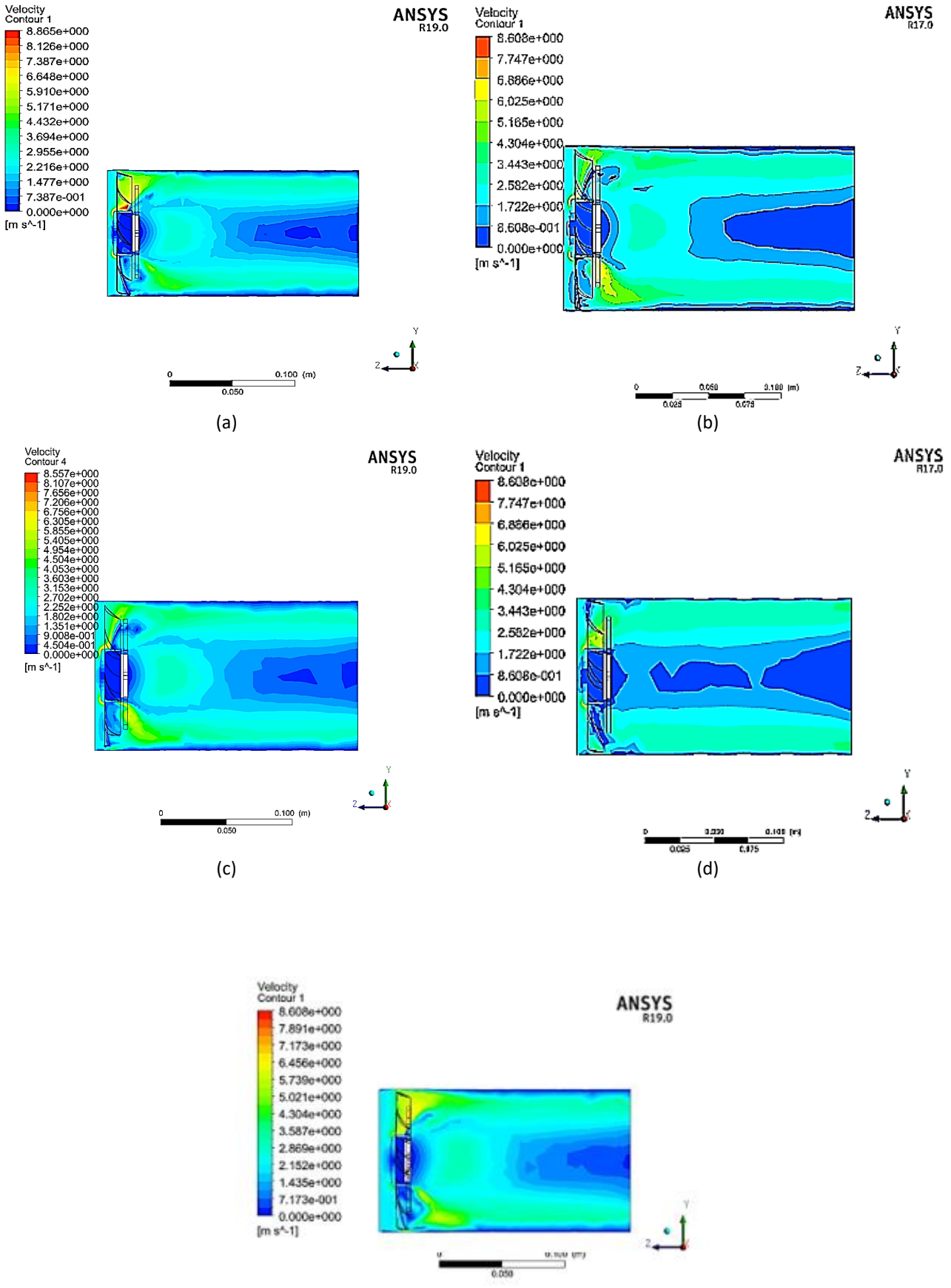

Fig. 11. Velocity contour for (a) a=35 (b) 30 (c) 28 (d) 26 and (e) 24˚C

In the normal flow direction just after the fan propeller, the highest twist angle 35° achieved the highest regularity in the velocity contour where the maximum efficiency of the fan can be obtained, in addition to that the fan body supports interference on the fan accelerated flow is relatively contradictive other than the other degrees twist angles as indicated below in Figure 12 (a)-(e). The twisting angle 24˚ effect has slowed the flow pattern more rapidly noticing that the flow between the fan blades has increased local velocity due to the increased blades edges contraction.

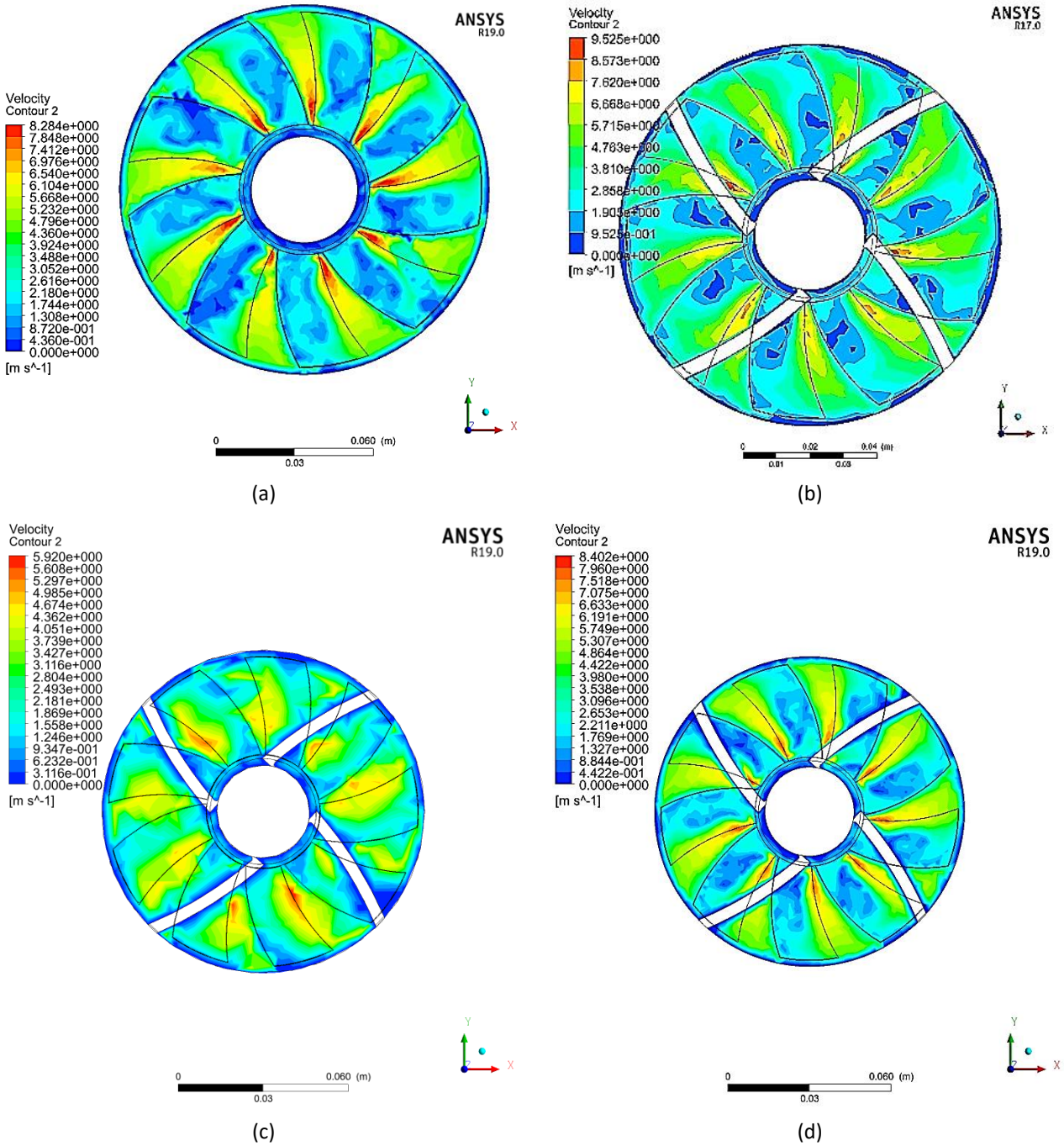

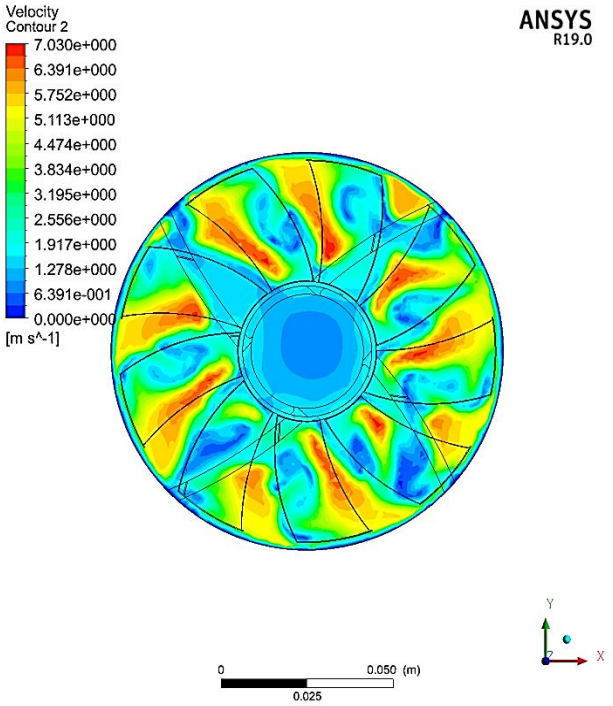

(e)

Fig. 12. Velocity contour for (a) a=35 (b) 30 (c) 28 (d) 26 and (e) 24˚C

In the square-shaped duct, the outcome the twist angle formal gives semi-analogy results for the prescribed blade tip angle effect illustrated in Figure 13 (a)-(e) but with a lower grade for the maximum obtained velocities, the uniformity of the perforated velocity contours are gradually stepped down noticing the end-wall corners zero-gradient velocity contours are eliminated. The reason for the gradually increased velocity near the blades tips as the twisting angle is increased is due to the increased differential flow pressure between the blades upper and lower surfaces.

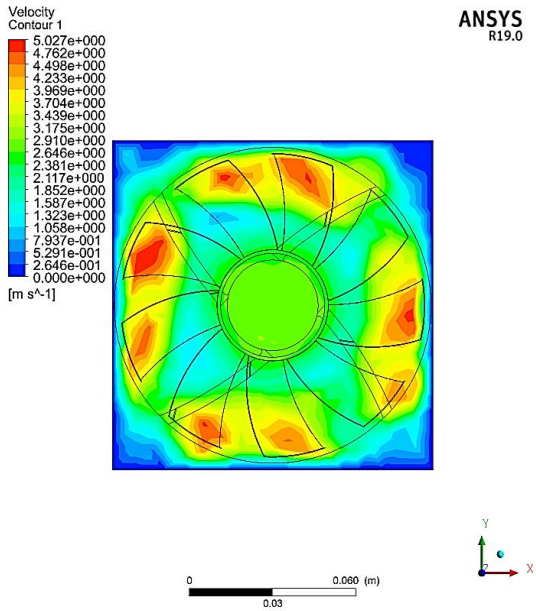

(a)

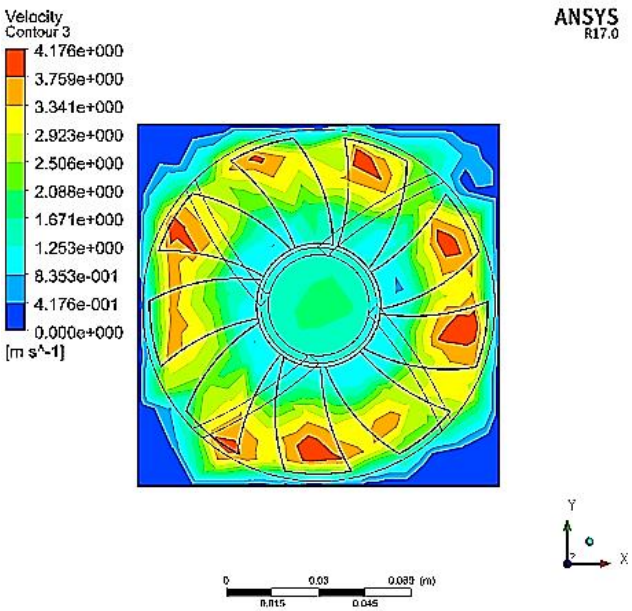

(b)

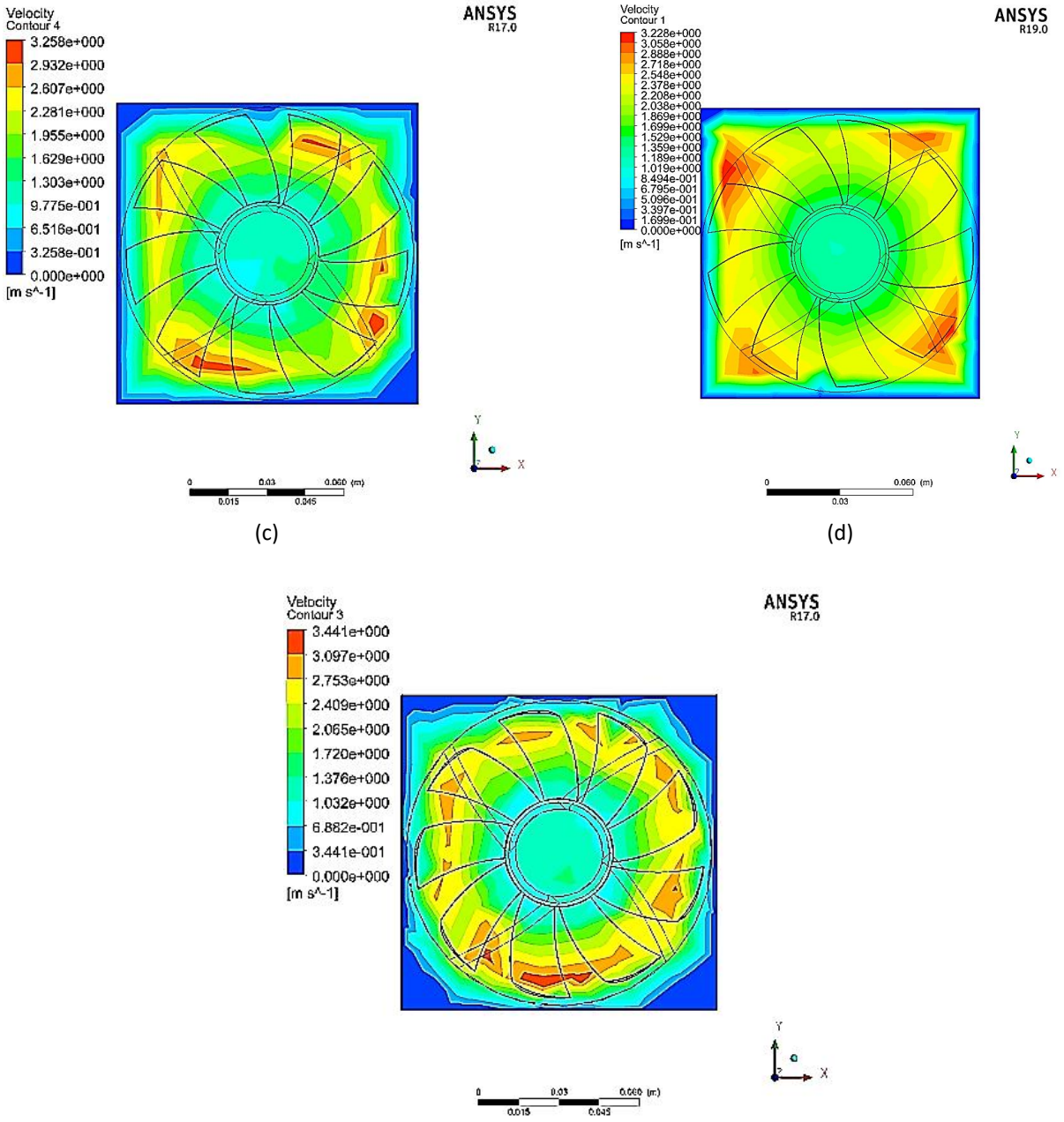

Fig. 13. Velocity contour for (a) a=35 (b) 30 (c) 28 (d) 26 and (e) 24˚C

5. Numerical Results Validation

The utilization of the (1/8)" probe Pitot tube for the numerical solution results validation focusing on the axial flow velocity at the specified locations are illustrated in Figure 14 and Figure 15, respectively. The first profile in Figure 14 shows a percentage error for the maximum velocity value profile inside the duct within 10% to 7% from the simulated results for the original fan blade profile with the default geometry parameters.

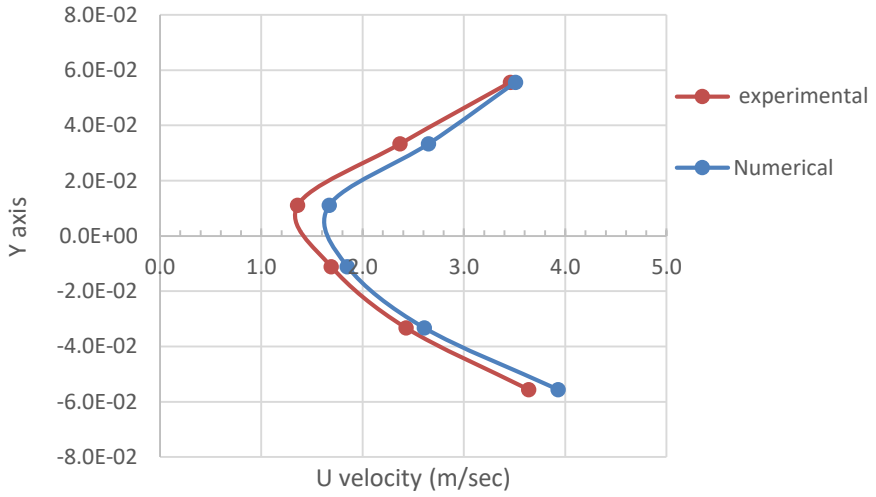

Fig. 14. Evaluated and measured axial velocity profile (0.5 cm) after the fan

The second oriented position results in Figure 15 indicates the longitudinal dropdown in the axial velocity downstream the fan position articulate better percentage error reaching 7% to 4%, respectively.

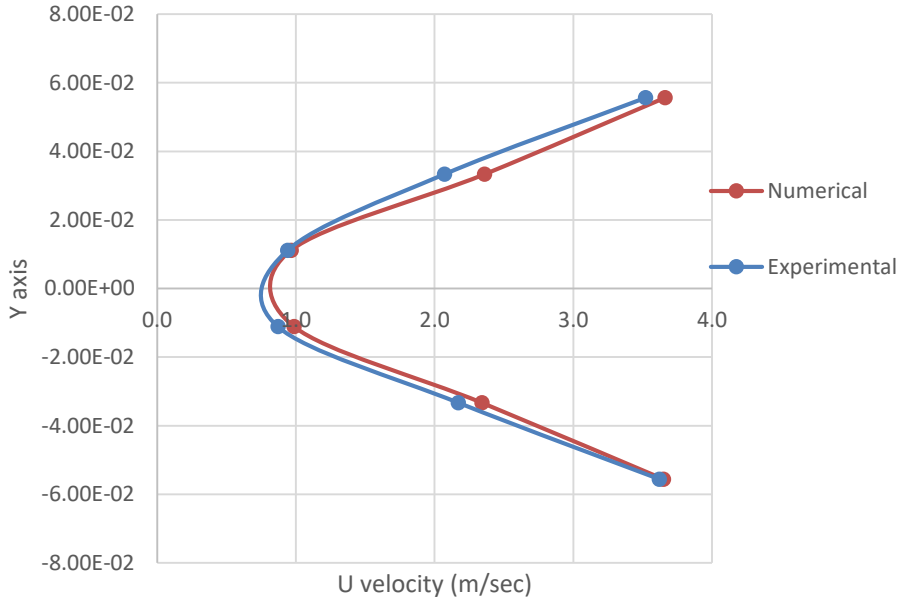

Fig. 15. Evaluated and measured axial velocity profile 3 cm after the fan

5. Grid Dependency Test

In order to ensure the achieved results dependency on the mesh statistical data, the mesh resolution is changed from its assigned value from (6e6) nodes and (4e6) elements to around (7e6) and (5e6), respectively. The achieved results shown in Figure 16 (a)-(b) indicate the small increased mesh concentration effect on the velocity contours.

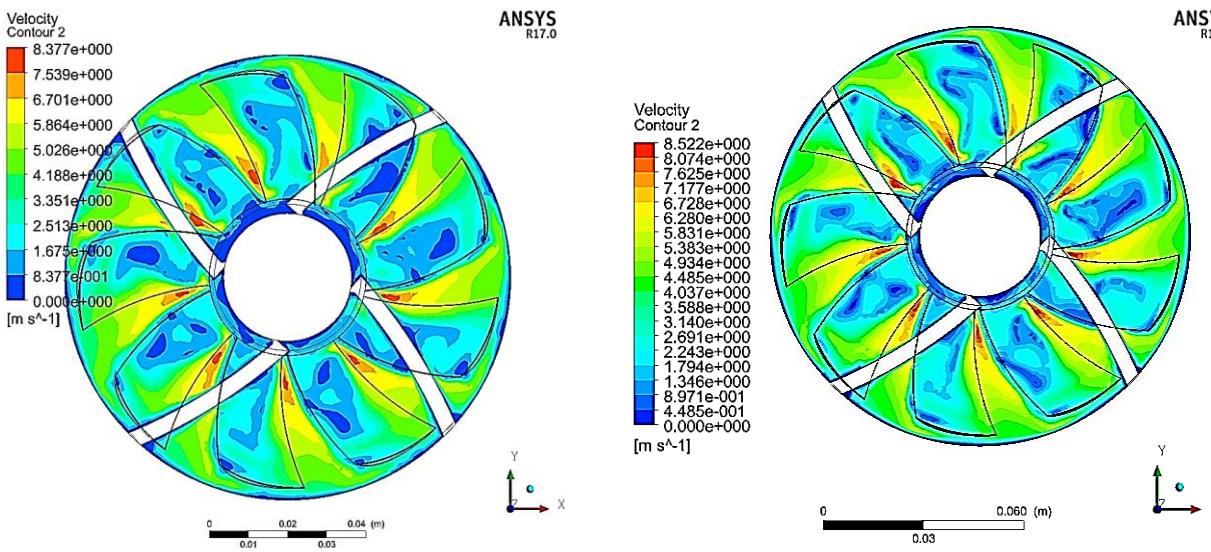

(a) (b)

Fig. 16. The (a) first and (b) second concentrated mesh results for IND 80 with increased height

6. Conclusions

It is concluded that the axial fan accelerating is more effective in the circular duct, the winglet incidence angle change from the vertical to the inclined position the flow disturbance is slightly increased due to its small tip height noticing that the vertical tip achieves a more stable near-wall velocity degradation in the longitudinal direction. The second conclusion is that the blade tip height increment will also reduce the turbulence wakes behind the fan propeller due to the reduction in the near-wall gap returning flow domain. The third investigated parameter which is the blade profile leading twisting angle where it's increased value will achieve more flow uniformity results to increase the fan accelerating efficiency.

Acknowledgement

I am very grateful for the valuable assistance that is submitted from Ass. Prof. Dr. Nabil N. Swadi in the precise sketching of the winglet fan using the SOLIDWORKS CAD.

References

[1] Nashimoto, Atsushi, Nobuyuki Fujisawa, Tsuneo Akuto, and Yuichi Nagase. "Measurements of aerodynamic noise and wake flow field in a cooling fan with winglets." *Journal of visualization* 7, no. 1 (2004): 85-92.

[2] Ye, Xuemin, Pengmin Li, Chunxi Li, and Xueliang Ding. "Numerical investigation of blade tip grooving effect on performance and dynamics of an axial flow fan." *Energy* 82 (2015): 556-569.

[3] Belferhat, S., S. M. A. Meftah, T. Yahiaoui, and B. Imine. "Aerodynamic Optimization of a Winglet Design." In *EPJ Web of Conferences*, vol. 45, p. 01010. EDP Sciences, 2013.

[4] Han, Shaobing, Jingjun Zhong, Huawei Lu, Xiaoxu Kan, and Ling Yang. "Effect of winglet geometry arrangement and incidence on tip clearance control in a compressor cascade." *Journal of Thermal Science* 23, no. 4 (2014): 381-390.

[5] Chan, Lee, Hyun Gwon Kil, Hyo Sang Kim, and Hwan Geol Yeo. "The performance improvement of axial flow fan with large tip clearance by using winglet." In *IOP Conference Series: Earth and Environmental Science*, vol. 186, no. 5, p. 012009. IOP Publishing, 2018.

[6] Beskales, S. A., Samir S. Ayad, M. G. Higazy, and O. E. Abdellatif. "The effect of tip end-blade geometry on the axial fans performance." In *Proceedings of the Eleventh International Conference of Fluid Dynamics, ICFD11-EG-4099, Alexandria, Egypt*. 2013.

[7] Jung, Jae Hyuk, and Won-Gu Joo. "Effect of tip clearance, winglets, and shroud height on the tip leakage in axial flow fans." *International Journal of Refrigeration* 93 (2018): 195-204.

[8] Bizjan, B., M. Milavec, B. Širok, F. Trenc, and M. Hočevar. "Energy dissipation in the blade tip region of an axial fan." *Journal of Sound and Vibration* 382 (2016): 63-72.
[9] Gavrilov, A. A., and V. Ya Rudyak. "Direct numerical simulation of the turbulent flows of power-law fluids in a circular pipe." *Thermophysics and Aeromechanics* 23, no. 4 (2016): 473-486.
[10] Volkov, K. N. "Near-wall modelling in computations of turbulent flows on unstructured grids." *Thermophysics and Aeromechanics* 14, no. 1 (2007): 107-123.
[11] Connolly, Brian J., Eric Loth, and C. F. Smith. "Unsteady Numerical Investigation of a Rectangular Diffusing S-duct with High Aspect Ratio." In *2018 AIAA Aerospace Sciences Meeting*, p. 2130. 2018.
[12] Demenkov, A. G., and G. G. Chernykh. "Numerical modeling of the swirling turbulent wake decay past a self-propelled body." *Thermophysics and Aeromechanics* 23, no. 5 (2016): 667-675.
[13] Sentyabov, A. V., A. A. Gavrilov, and A. A. Dekterev. "Investigation of turbulence models for computation of swirling flows." *Thermophysics and aeromechanics* 18, no. 1 (2011): 73.
[14] Kunya, Bashir Isyaku, Clement Olaloye Folayan, Gyang Yakubu Pam, Fatai Olukayode Anafi, and Nura Mu'az Muhammad. "Performance study of Whale-Inspired Wind Turbine Blade at Low Wind Speed Using Numerical Method." *CFD Letters* 11, no. 7 (2019): 11-25.